Green Chemistry

PAPER

View Article Online
View Journal | View Issue

Cite this: *Green Chem.*, 2017, **19**, 1911

Blue light mediated C–H arylation of heteroarenes using TiO_2 as an immobilized photocatalyst in a continuous-flow microreactor†

David C. Fabry,[a] Yee Ann Ho,[a] Ralf Zapf,[b] Wolfgang Tremel,[c] Martin Panthöfer,[c] Magnus Rueping*[a] and Thomas H. Rehm*[b]

Received 15th February 2017,
Accepted 16th March 2017

DOI: 10.1039/c7gc00497d

rsc.li/greenchem

Titanium dioxide was applied as an immobilized photocatalyst in a microstructured falling film reactor for the continuous-flow C–H arylation of heteroarenes with aryldiazonium salts as the starting material. Detailed investigations of the catalyst and a successful long-term run proved its excellent usability for this process. Very good yields up to 99% were achieved with broad substrate scope and were compared with batch synthesis. The transfer to the continuous-flow mode revealed an impressive boost in reactor performance solely resulting from the improved irradiation and contact of the catalyst, substrate and light.

Introduction

Titanium dioxide has proved its potential as a heterogeneous photocatalyst for various applications in chemical synthesis.[1] The outstanding chemical and photochemical stabilities of TiO_2 allow, in combination with its high availability, low cost and non-toxicity, its use in advanced oxidation processes (AOP) for the mineralization of toxic compounds in wastewater.[2] In contrast to degradation processes TiO_2 has also attracted considerable interest as a photocatalyst for fine chemical syntheses.[3] Alcohol,[4] amine[5] and thiol[6] oxidation to aldehydes, imines and disulfides, respectively, are known as well as various methods for C–C[7] and C–heteroatom[8,9] bond forming reactions. Hydrogenation reactions, of *e.g.* nitro arenes to the respective amines,[10] or the cyclisation of L-lysine to L-pipecolinic acid,[11] have been performed with pure TiO_2 or with Pt nanoparticles as a co-catalyst attached to the TiO_2 particle surface. Particularly the use of co-catalysts with TiO_2 has been explored in recent times in order to overcome the limiting UV absorption range of pure TiO_2 and enter the visible light region for a milder and even more sustainable synthetic photo-process.[12–15] The *in situ* surface modification of TiO_2 is another possibility to enhance the absorption range of the photocatalyst. As recently shown by Rueping *et al.*, the TiO_2 surface catalysed formation of a TiO_2 azoether from aromatic diazonium salts results in a strong light absorption in the blue region with a maximum of approx. 450 nm.[16] Irradiating this substrate–catalyst combination results in the formation of aryl radicals, which efficiently add to heteroarenes like furan or thiophene available in the reaction solution.

In parallel to the development of photochemically catalysed reactions with visible light, continuous-flow technology has become one important tool for photochemists.[17–19] Microtubular-based reactors are a commonly used reactor type for photochemical transformations.[20–22] They are equipped with thin light transparent capillaries having an inner diameter of less than a millimetre. Energy-efficient light emitting diodes are recommended for the wavelength-selective irradiation of the liquid thin film of the reaction solution inside the capillary.[23,24] In contrast to batch photo-reactions continuous-flow reactors allow the exact control of the irradiation time by the flow rate of the reaction solution being pumped through the capillary. This advantage minimizes detrimental effects on the product formation due to over-irradiation. Besides these advantages microstructured reactors also allow an intense mixing of liquid or gas–liquid phases inside the micro-sized channels yielding efficient mass transfer and accelerated reactions.[25–28] The use of solid phases like heterogeneous photocatalysts needs another reactor design. Flexible capillaries are replaced by stiff microchannels made of inert polymers or glass. A heterogeneous catalyst material can be then coated to the walls of the microchannels.[29] This approach is usually used for reaction screening and synthesis development

[a]RWTH Aachen University, Institute of Organic Chemistry, Landoltweg 1, 52074 Aachen, Germany. E-mail: magnus.rueping@rwth-aachen.de; Fax: +49 241 8092665
[b]Fraunhofer ICT-IMM, Carl-Zeiss-Straße 18-20, 55129 Mainz, Germany. E-mail: thomas.rehm@imm.fraunhofer.de; Tel: +49 6131 990 195
[c]Johannes Gutenberg University Mainz, Institute of Inorganic Chemistry and Analytical Chemistry, Duesbergweg 10-14, 55128 Mainz, Germany

†Electronic supplementary information (ESI) available: Catalyst preparation and immobilisation, surface roughness, TEM, nitrogen physisorption, XRD, SEM, EDX, lab plant description and flow chart, synthesis of aryldiazonium salts, ^{19}F NMR analysis during long-term run, and product characterization: ^{1}H-, ^{13}C-, and ^{19}F-NMR spectroscopy. See DOI: 10.1039/c7gc00497d

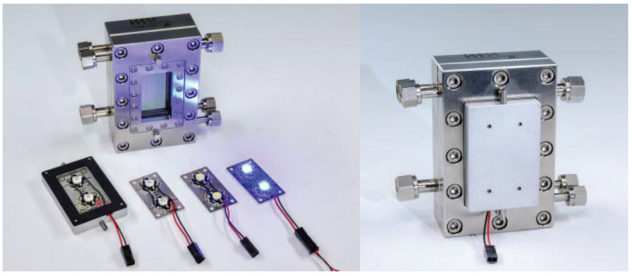

Fig. 1 FFMR as the key element of the lab plant with a royal blue LED array in a heat sink magnetically fixed to the top plate of the microreactor (© Fraunhofer ICT-IMM).

in chip reactors with a small internal volume and low flow rate on the μL min^{-1} scale.[30–32]

For scale-up of a well-explored batch photo-reaction and its transfer into continuous-flow mode a larger reactor type is necessary, like the microstructured falling film reactor (FFMR) (Fig. 1). The design and working principle of the FFMR allows the formation of liquid thin films in open stainless steel microchannels with a thin film thickness below 100 μm and flow rates of 1 mL min^{-1} for the standard reactor version and up to 10 mL min^{-1} for the large reactor version (for more details, see the ESI†).[33–36] The FFMR has already been used for photochemical reactions like photochlorinations[37] and dye-sensitized singlet oxygen formation.[38,39] Very recently the FFMR was evaluated in detail for the dye-sensitized photooxygenation of 1,5-dihydroxynaphthalene to Juglone.[40]

In the work presented here the FFMR technology is used for the first time with a heterogeneous photocatalyst immobilized inside the microchannels. Based on previous work by Rueping *et al.* on the TiO_2 catalyzed C–H arylation of heteroarenes with diazonium salts as the starting material, this reaction is transferred from small scale batch to continuous-flow mode in the FFMR with TiO_2 as an immobilized photocatalyst in stainless steel microchannels. Besides catalyst analysis a wide range of aryldiazonium salts are investigated with furan, thiophene and pyridine as heteroarenes including a long-term run. Calculation of the specific reactor performance proves a considerable boost in the performance and superiority of continuous-flow synthesis in the FFMR against batch synthesis.

Results and discussion

Catalyst immobilisation and analysis

For all experiments reaction plates were used with 32 microchannels and a channel architecture of 600 μm in width, 200 μm in depth and 78 mm in length (Fig. 2, left). TiO_2 (24 mg, anatase modification) was immobilized as a catalytically active metal oxide as described in the Experimental section (*vide infra*). Cleaning of the reaction plate with citric acid and heat treatment at 800 °C prior to the immobilization of the metal oxide with poly-vinyl alcohol as a binder enables strong adhesion of the catalyst material to the stainless steel

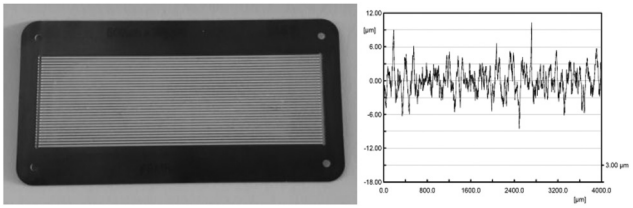

Fig. 2 FFMR reaction plate with TiO_2 immobilized in 32 microchannels (left) and the roughness of the catalyst material inside a microchannel (right).

surface.[41] The applied method allows the immobilisation of a thin TiO_2 layer solely in the microchannels of the reaction plate. The surface roughness of the calcined catalyst material was investigated for five measuring lengths of 4 mm along the bottom of one microchannel. The arithmetical mean deviation of the roughness profile is R_a = 1.84 μm, and the average surface roughness is R_z = 13.71 μm (Fig. 2, right and ESI†). The data from these experiments indicate a constant roughness with an equal distribution of catalyst material on the wall of the surveyed microchannel. The surface roughness allows the generation of turbulence in the liquid thin film for efficient contact of the liquid stream with the catalyst surface.

The specific surface area and the pore diameter of the catalyst material were analysed before and after calcination (see the ESI† for details). Prior to the thermal treatment TiO_2 powder had a specific surface area of 157.11 m^2 g^{-1} with a median pore diameter of 6.6 nm. After wet catalyst preparation and calcination at 450 °C the specific surface area was reduced to 118.93 m^2 g^{-1}, whereas the median pore diameter had increased to 8.7 nm. These values obtained with the BET and BJH methods show a typical trend of mesoporous TiO_2 upon thermal treatment.[42] Transmission electron microscopy (TEM) was used to visualize the particle size of TiO_2 before and after calcination. Large agglomerates are observed in both cases. Before temperature treatment TiO_2 particles show a regular dimension within the larger agglomerates (Fig. 3, left). After thermal treatment TiO_2 particles tend to stick together to larger structures within the agglomerates (Fig. 3, right). This appearance can be attributed to the adhesion between the particles upon interaction with the binder from catalyst preparation.

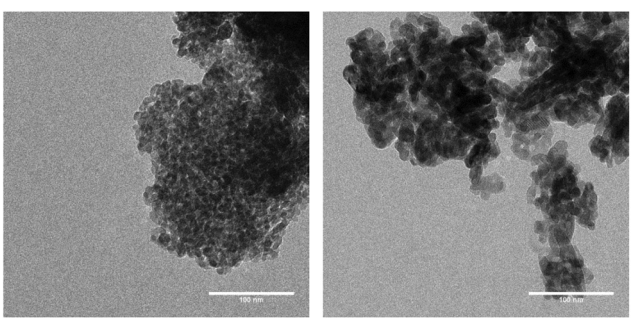

Fig. 3 TEM images of TiO_2 particles before (left) and after (right) calcination at 450 °C (length scale: 100 nm).

Further analysis of TiO_2 was carried out using X-ray diffraction (XRD) in order to gain insight into the crystal modification of nano-powderous TiO_2 before and after thermal treatment. All patterns exhibit reflections due to the anatase as well as the rutile modification of TiO_2, the latter being the minor component (Fig. 4). The reflection profiles of the anatase phase are broad as expected for nanoscale materials, yet the tips of the reflections are too sharp. Thus the anatase component was modelled using two phases of identical crystallographic data, but with different crystallite sizes and mass ratios. In this model the sharp tips of the reflection profiles are due to a minor component of approx. 5 wt% with a crystallite size larger than 100 nm. In this crystallite size regime reflection broadening due to the crystallite size and the broadening due to the diffractometer technical limits become comparable, thus a more precise value of the crystallite size of the minor phase cannot be determined from laboratory diffractometer data. Importantly, calcination changes the TiO_2 catalyst only negligibly, but the composition and crystallite size before and after calcination are virtually the same.

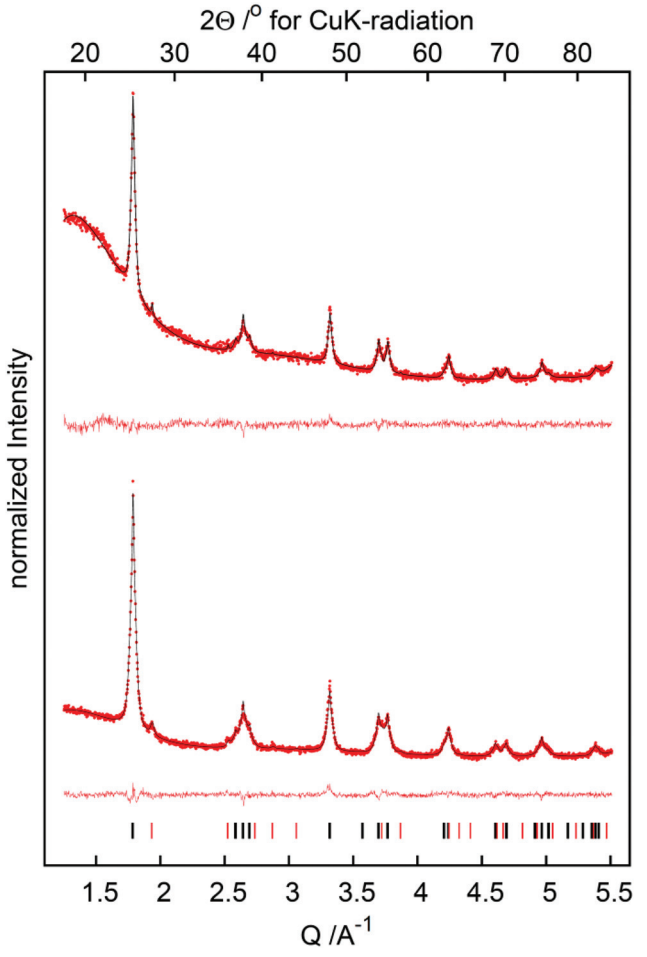

Fig. 4 X-ray powder diffraction patterns of the TiO_2 before (bottom) and after (top) calcination (red dots: experimental data, black line: fit, red line: difference curve; ticks indicate the reflection positions of the anatase (black) and rutile (red) phases, respectively).

Scanning electron microscopy was carried out to investigate the surface structure of immobilized TiO_2 before and after its use in the microreactor (Fig. 5). Despite a little change in colour from off-white to slightly yellowish, neither on the submicrometre scale nor on a larger scale any changes of the surface structure have been observed after intense use of the TiO_2 coated plate for all runs (see the ESI† for images with lower magnification).

In conjunction with SEM analysis energy dispersive X-ray (EDX) analysis was performed as well to check the composition of the catalyst material in the microchannels before and after its use in flow synthesis (Table 1 and ESI†). In both cases titanium and oxygen represent the major share of the detected elements in the correct ratio for TiO_2, whereas the oxygen share is slightly higher in the unused sample. This portion as well as the carbon content of 2.55 atom% can be attributed to residues of the binder poly(vinyl alcohol) from catalyst preparation. The used sample shows a significant carbon and fluorine content of 3.41 atom% and 3.20 atom%, respectively. Both elements result from the last experiments performed with trifluoromethylated benzenediazonium salts (*vide infra*). A low content of iron with 0.62 atom% and 1.05 atom%, respectively, most likely results from the stainless steel reaction plate as a catalyst carrier.

Lab plant design and reactor integration

The FFMR is part of an integrated multi-purpose lab plant for different reactor types (FFMR and tube-in-tube flow reactor) (Fig. 6). The heat exchanger of the FFMR is connected to a water-filled thermostat for maintaining the temperature of the reaction plate at 20 °C (see the ESI† for details of the flow

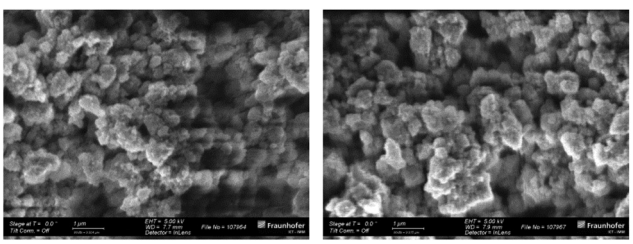

Fig. 5 SEM images of the TiO_2 surface in the microchannels before (left) and after (right) use in the FFMR (length scale: 1 μm).

Table 1 Element composition of catalyst material inside the microchannels as analysed by EDX

Element	Before use in FFMR, atom%	After use in FFMR, atom%
C	2.55	3.41
O	70.06	65.30
F	—	3.20
P	0.35	0.23
S	0.12	—
Ti	26.30	26.67
Cr	—	0.13
Fe	0.62	1.05

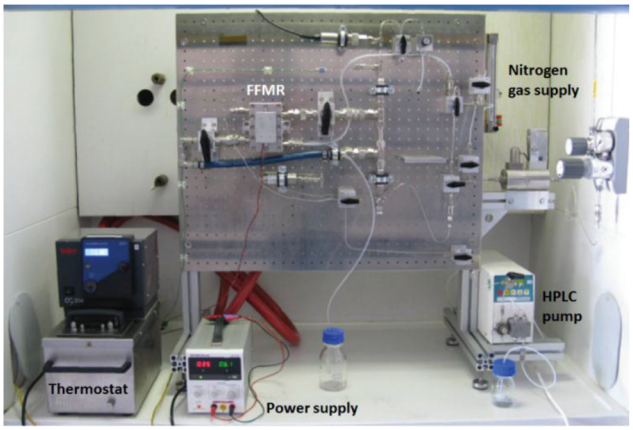

Fig. 6 FFMR lab plant with a HPLC pump, thermostat, nitrogen gas supply and power supply of the LED array.

chart). This external cooling is necessary since prolonged LED irradiation can lead to heating of the reaction plate and solvent evaporation in the microchannels which results in falsification of the residence time of the reaction solution in the microreactor. The starting material solution is pumped with a HPLC pump into the reactor at a flow rate f_{liq} = 0.5 mL min^{-1}. A nitrogen gas stream is fed in counter-flow to the liquid stream into the FFMR. This inert gas flow of approx. 10 mL min^{-1} was used to support the self-draining of the reactor. All LEDs (actinic blue, royal blue, cold-white) used for the experiments are installed on an aluminium heat sink, which can be fixed magnetically in front of the inspection window of the FFMR (Fig. 1).

Reaction evaluation and substrate scope

The first set of experiments was performed with 4-fluorobenzenediazonium salt **1a** and furan as a heterocycle. In order to investigate the necessity and type of photocatalyst several runs were performed with different metal oxides using royal blue light (455 nm) at a flow rate f_{liq} = 0.5 mL min^{-1} (Table 2). In the case of TiO_2 a yield of 79% was obtained (entry 1), whereas for ZnO and Bi_2O_3 only low yields could be achieved (entries 2 & 3).[43] In the case of a blank reaction plate without metal oxide no reaction took place (entry 4). The impact of the light source was investigated as well with the reaction plate carrying TiO_2. The use of cold-white light (6500 K, entry 5) and actinic blue (410 nm, entry 6) as well as the absence of light as the blank test (entry 7) was ineffective compared to royal blue light, which provided a maximum light intensity at the absorption range of the photoactive TiO_2 azoether at approx. 450 nm.[16] Therefore, all further experiments were performed with royal blue light for irradiation and TiO_2 as the catalyst material. Under these conditions the furan series was completed with three more diazonium salt derivatives showing approximately the same or better yields compared to the batch synthesis (entries 8–10, Table 2).

The next set of experiments was performed with thiophene as the heterocycle for C–H arylation (Table 3). In the case of **6b** the same yield of 72% was obtained by flow and batch synthesis. The nitro derivative **6c**, however, gave a considerably lower yield of 42% compared to 83% in the batch synthesis. A moderate yield of 45% was achieved for the trifluoromethylated compound **6d** (Table 3). Pyridine was used as the last heterocycle. Surprisingly, the pyridine series yielded in continuous-flow far better results than *via* the batch synthesis. In the case of **7b** 99% yield was obtained compared to 79% in batch. The same trend was observed for **7c** with 85% yield in flow synthesis compared to 53% in batch. Therefore, a broader substrate scope was investigated. Except for **7e** (p-CF_3) with 75% yield excellent yields of up to 99% were obtained for all other pyridine compounds (Table 3). To complete the substrate scope, the precursor of dantrolene, an API for muscle relaxation, was synthesized as well in continuous-flow mode (Table 3, framed). Furfural (**8**) was used as a heterocycle with **1c** as a diazonium salt under standard reaction conditions with f_{liq} = 0.5 mL min^{-1}, T = 20 °C and royal blue light with TiO_2 as a photocatalyst. A slightly lower yield of 65% was achieved for **9** in continuous-flow mode compared to 68% in batch. The conversion of **9** with 1-aminohydantoin hydrochloride provided dantrolene in an excellent yield of 92% (see the ESI†).

Table 2 Evaluation of the reaction conditions and substrate scope for furan series[a]

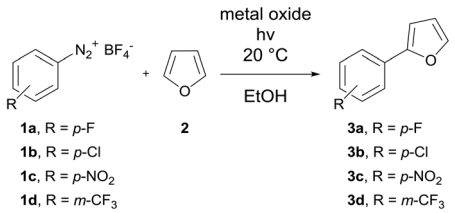

1a, R = *p*-F
1b, R = *p*-Cl
1c, R = *p*-NO_2
1d, R = *m*-CF_3

2

3a, R = *p*-F
3b, R = *p*-Cl
3c, R = *p*-NO_2
3d, R = *m*-CF_3

Entry	Substrate	Metal oxide[b]	Light source[c]	Yield: flow synthesis[d] (%)	Yield: batch synthesis[e] (%)
1	**1a**	TiO_2	Royal blue	79	96
2	**1a**	ZnO	Royal blue	<10	—
3	**1a**	Bi_2O_3	Royal blue	<10	—
4	**1a**	—	Royal blue	0	—
5	**1a**	TiO_2	Cold-white	<10	—
6	**1a**	TiO_2	Actinic blue	<10	—
7	**1a**	TiO_2	—	0	—
8	**1b**	TiO_2	Royal blue	99	94
9	**1c**	TiO_2	Royal blue	87	90
10	**1d**	TiO_2	Royal blue	91	—

[a] Reaction conditions: 5 mmol **1a–d** in 100 mL EtOH/furan (1 : 1, v/v); T = 20 °C; f_{liq} = 0.5 ml min^{-1}. [b] Amount of immobilized metal oxide: $m(TiO_2)$ = 24 mg, m(ZnO) = 24 mg, $m(Bi_2O_3)$ = 27 mg. [c] Electrical power $P_{ele} \approx$ 2.4 W. [d] Yield after chromatographic purification. [e] See ref. 16.

Long-term run

The long-term run was performed with 4-trifluoromethylbenzene diazonium salt (**1e**) in EtOH and pyridine as heteroarenes. Standard reaction conditions were applied as well in this experiment with T = 20 °C, f_{liq} = 0.5 mL min^{-1}, royal blue light and TiO_2 immobilized in the microchannels. During the

Table 3 Reaction conditions and substrate scope for thiophene and pyridine series[a]

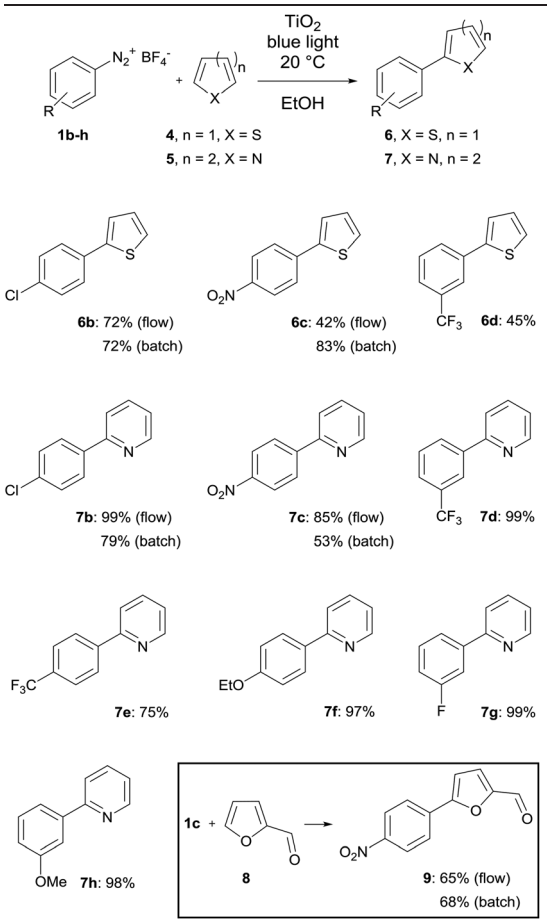

[a] Reaction conditions: 5 mmol **1b–h** in 100 mL EtOH/thiophene or pyridine (1 : 1, v/v); T = 20 °C; f_{liq} = 0.5 ml min^{-1}; amount of immobilized metal oxide: $m(TiO_2)$ = 24 mg; yield of continuous-flow synthesis after chromatographic purification; yield of batch synthesis, see ref. 16.

complete run time of 180 min nine samples were taken from the reactor outlet and mixed with 4-trifluoromethylbenzyl alcohol as the internal standard (^{19}F NMR (56 MHz) δ = −65.99; s, 3F) in DMSO-d$_6$. Over the complete run time the process was performing constant with a mean conversion of 77%, which is in good agreement with the yield of 75% achieved with the synthesis during substrate scope evaluation (Fig. 7). The NMR spectra revealed only the product **7e** (^{19}F NMR (56 MHz) δ = −66.44) and the diazoether of **1e** with ethanol being the intermediate compound of the synthesis (^{19}F NMR (56 MHz) δ = −66.28). It has to be pointed out that reaction evaluation and long-term run has been performed with solely one plate with immobilized TiO_2. This fact proves the exceptional durability and reusability of the immobilized catalyst.

Flow reactor performance

The specific reactor performance L is an important parameter to characterize chemical processes performed using different

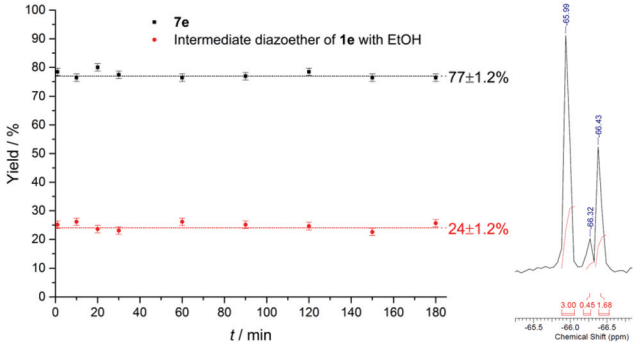

Fig. 7 Constant yields for **1d** during long-term run over 180 minutes (left) and part of the ^{19}F NMR spectra of the sample taken after 30 minutes (right).

reactor systems. In the case of a batch reactor system the specific reactor performance L_{batch} is usually described by:[44]

$$L_{batch} = \frac{c_{starting\,material} \times Y_{product}}{t_R + t_D}\ [mol\,L^{-1}\,min^{-1}] \quad (1)$$

with $c_{starting\ material}$ as the molar concentration of the starting material, $Y_{product}$ as the yield of the desired product and t_R as the reaction time. The dead time t_D can be assumed for filling the reaction vial, starting the reaction and quenching the reaction afterwards. The specific reactor performance of the FFMR L_{FFMR} can be calculated by:[44]

$$L_{FFMR} = \frac{c_{starting\,material} \times Y_{product}}{\tau}\ [mol\,L^{-1}\,min^{-1}] \quad (2)$$

with τ as the residence time of the reaction solution in contact with the catalyst material. The residence time τ can be calculated by:[45]

$$\tau = \frac{N \times V_c}{f_{liq}} = \frac{N \times W \times L \times \delta}{f_{liq}}\ [s] \quad (3)$$

with N as the number of microchannels on the reaction plate, V_c as the irradiated volume of the reaction solution in one microchannel, W as the width of a microchannel, L as the microchannel length, δ as the liquid thin film thickness and f_{liq} as the flow rate of the reaction solution. The liquid thin film thickness δ can be expressed by the Nusselt equation:[45,46]

$$\delta = \sqrt[3]{\frac{3 \times f_{liq} \times \mu_{liq}}{N \times \rho_{liq} \times W \times g}}\ [\mu m] \quad (4)$$

with μ_{liq} as the dynamic viscosity of the reaction solution, ρ_{liq} as the density of the reaction solution and g as the gravitational constant. The conversion of 4-chlorobenzenediazonium salt (**1b**) with pyridine to 2-(4-chlorophenyl)pyridine (**7b**) was chosen for comparing batch and continuous-flow synthesis. In Table 4 all necessary data are compiled for the calculation of the specific reactor performance of the batch system and the continuous-flow reactor. In the case of the batch synthesis a specific reactor performance of L_{batch} = 5.4 × 10^{-5} mol L^{-1} min^{-1} was calculated. For the continuous-flow synthesis in the FFMR a specific

Table 4 Data for and results of the calculation of the specific reactor performance L

	Batch[a]	Flow	Unit
Molar concentration $c_{\text{starting material}}$	0.05	0.05	mol L^{-1}
Yield Y_{product}	79%	99%	—
Number N of microchannels	—	32	—
Microchannel width, W	—	600	μm
Channel length, L	—	78[c]	mm
Gravitational constant, g	—	9.81	m s^{-2}
Liquid flow rate, f_{liq}	—	0.5	mL min^{-1}
Dynamic viscosity, μ	—	0.8839[d]	g mL^{-1}
Density, ρ	—	0.8910[d]	mPa s
Reaction time, t_R	720	—	min
Dead time, t_D	15[b]	—	min
Liquid thin film thickness, δ	—	50.9	μm
Residence time, τ	—	9.1	s
Specific reactor performance, L	5.4×10^{-5}	0.32	mol L^{-1} min^{-1}

[a] Data extracted from ref. 16. [b] Estimated dead time. [c] The full length of a microchannel is used for the calculation, since the dual role of TiO_2 (diazoether formation and photocatalysis) is not only limited to the directly and fully irradiated length of 54 mm. [d] Data extracted from ref. 47.

reactor performance of L_{FFMR} = 0.32 mol L^{-1} min^{-1} was calculated. The extreme performance increase by a factor of approx. 6000, solely by switching from batch to continuous-flow mode, can be attributed to the following reasons. The FFMR offers a strongly improved irradiation of the reaction solution compared to the batch synthesis. The royal blue LED array provides solely the light exactly matching to the absorption range of the TiO_2 diazoether. During the process the volume of the reaction solution inside the microchannels is quite small (approx. 0.08 mL) and in intense contact with the fully irradiated catalyst surface. This efficient combination is in clear contrast to the batch synthesis where the complete catalyst suspension volume is irradiated by a rather unspecific light source.

Conclusions

For the first time the falling film microreactor technology was successfully applied to a photochemically catalysed reaction with TiO_2 as an immobilized photocatalyst in the microchannels of a continuous-flow reactor. A wide variety of arenediazonium salts were used as the starting material for blue light mediated C–H arylation of heteroarenes in continuous-flow mode. Furan, thiophene and pyridine as well as furfural were converted into the desired products with good to excellent yields up to 99%. A long-term run over 180 min was successfully performed as well in order to demonstrate the catalyst performance. Detailed XRD, SEM and EDX analyses of the catalyst material before and after calcination and its use in the microreactor, respectively, proved the excellent stability and usability of TiO_2 as an immobilized photocatalyst in a continuous-flow microreactor. The transfer of the C–H arylation of heteroarenes from batch mode to continuous-flow revealed a boost in the specific reactor performance up to a factor of 6000. This strong increase can be attributed to the improved irradiation and substrate–catalyst–light interaction on the microstructured surface of the continuous-flow reactor. These results clearly show the major advantages for photochemistry when performed in a microstructured environment.

Experimental

Catalyst preparation and immobilization

A slurry-washcoat process was used for the immobilization of catalyst material on the FFMR reaction plate. The preparation of TiO_2, ZnO and Bi_2O_3 washcoats was carried out according to literature procedures.[41,48] The method is exemplified here for TiO_2. 2.5 g of poly(vinyl alcohol) (PVA) used as a binder (Sigma Aldrich, Mowiol 40–88) were mixed with 42.5 mL of distilled water and stirred at 65 °C until PVA had completely dissolved (approx. 2–3 h). 5 g of TiO_2 (Alfa Aesar, 45603, anatase modification) and 0.375 g concentrated acetic acid were added to the solution and stirred for 3 h at 65 °C, and finally at room temperature for 2–3 days, until the suspension became homogeneous and dense.

All reaction plates were cleaned with citric acid solution (10 wt% in water) under ultrasound treatment. After rinsing the cleaned plates with distilled water, they were heated in an oven at 800 °C. Prior to the deposition of the washcoat in the microchannels, the area on the reaction plate not to be coated with a catalyst was covered with an adhesive tape. Afterwards the microchannels were completely filled with the prepared suspension and the excess of the suspension was wiped off. After drying at room temperature in air, the coated plates were calcined at 450 °C for 6 h.

Catalyst analysis

The surface roughness of the catalyst layer inside the microchannels was measured with a NanoFocus AF 2000. The surface area and the pore diameter of the catalyst material were determined before and after calcination. Low temperature nitrogen physisorption was performed with Sorptomatic 1990 (Carlo Erba Instruments) automatic apparatus. The obtained information was used for the calculations of the surface area and the pore diameter by applying the BET and BJH methods. Transmission electron microscopy (TEM) images were recorded with a Zeiss Libra® 120 on copper grids with a carbon thin film (CF300-CU, EM Science). X-ray powder diffraction (XRD) patterns were recorded from powders prepared between two stripes of 3 M Scotch tape using a Siemens D5000 equipped with a Ge (111) monochromator (Huber 611 Guinier monochromator) and a Braun M50 position sensitive detector in transmission mode. Scanning electron microscopy (SEM) images were taken with a Zeiss Leo 1550 VP Field Emission Scanning Electron Microscope. The reaction plates containing TiO_2 were scanned without any sample preparation. The acceleration voltage was 5.00 kV, and the working distance was

between 7.7 and 8.0 mm. Energy Dispersive X-ray (EDX) analysis was performed with an Oxford INCA II setup.

General procedure for the TiO_2 catalyzed arylation in continuous-flow

Aryldiazonium tetrafluoroborates **1a–h** were synthesized according to literature procedures (for details, see the ESI†). The appropriate salt was dissolved in a solvent mixture of EtOH and the corresponding heterocycle (furan, thiophene, pyridine or furfural, v : v 1 : 1, 50 mM). The resulting mixture was stirred until complete solvation of the diazonium salt. Then, the mixture was pumped into the falling film microreactor for collapsing down into the microchannels. As soon as the reaction solution equally rinsed all microchannels irradiation was started by switching on the LED array connected to the FFMR. The crude reaction mixture was collected and filtered over a short plug of silica and flushed with ethyl acetate. If necessary, the final products were further purified using flash column chromatography on silica gel (eluent cyclohexane/ethyl acetate).

Acknowledgements

T. H. R. would like to thank Dr Raphael Thiermann for TEM analysis, Anja Himmelsbach for SEM and EDX analysis and Gitta Hasert for nitrogen physisorption analysis (all Fraunhofer ICT-IMM). This research has received funding from the European Research Council under the European Union's Seventh Framework Programme (FP/2007-2013)/ERC Grant Agreement no. 617044 (SunCatChem).

Notes and references

1 Y. Shiraishi and T. Hirai, *J. Photochem. Photobiol., C*, 2008, **9**, 157–170.
2 M. Chong, B. Jin, C. Chow and C. Saint, *Water Res.*, 2010, **44**, 2997.
3 N. Hoffmann, *Aust. J. Chem.*, 2015, **68**, 1621–1639.
4 A. Molinari, M. Montoncello, H. Rezala and A. Maldotti, *Photochem. Photobiol. Sci.*, 2009, **8**, 613–619.
5 N. Li, X. Lang, W. Ma, H. Ji, C. Chen and J. Zhao, *Chem. Commun.*, 2013, **49**, 5034–5036.
6 C. Bottecchia, N. Erdmann, P. Tijssen, L.-G. Milroy, L. Brunsveld, V. Hessel and T. Noël, *ChemSusChem*, 2016, **9**, 1781–1785.
7 C. Vila and M. Rueping, *Green Chem.*, 2013, **15**, 2056–2059.
8 V. Bhat, P. Duspara, S. Seo, N. Bakar and M. Greaney, *Chem. Commun.*, 2015, **51**, 4383–4385.
9 M. Rueping, J. Zoller, D. Fabry, K. Poscharny, R. Koenigs, T. Weirich and J. Mayer, *Chem. – Eur. J.*, 2012, **18**, 3478–3481.
10 G. Palmisano, E. García-López, G. Marcí, V. Loddo, S. Yurdakal, V. Augugliaro and L. Palmisano, *Chem. Commun.*, 2010, **46**, 7074–7089.
11 B. Pal, S. Ikeda, H. Kominami, Y. Kera and B. Ohtani, *J. Catal.*, 2003, **217**, 152–159.
12 S. Füldner, R. Mild, H. Siegmund, J. Schroeder, M. Gruber and B. König, *Green Chem.*, 2010, **12**, 400–406.
13 M. Cherevatskaya, M. Neumann, S. Füldner, C. Harlander, S. Kümmel, S. Dankesreiter, A. Pfitzner, K. Zeitler and B. König, *Angew. Chem., Int. Ed.*, 2012, **51**, 4062–4066.
14 X. Lang, J. Zhao and X. Chen, *Angew. Chem., Int. Ed.*, 2016, **55**, 4697–4700.
15 X. Lang, W. Hao, W. Leow, S. Li, J. Zhao and X. Chen, *Chem. Sci.*, 2015, **6**, 5000–5006.
16 J. Zoller, D. Fabry and M. Rueping, *ACS Catal.*, 2015, **5**, 3900–3904.
17 D. Cambié, C. Bottecchia, N. Straathof, V. Hessel and T. Noël, *Chem. Rev.*, 2016, **116**, 10276–10341.
18 T. Rehm, in *Flow Chemistry - Applications*, ed. F. Darvas, G. Dorman and V. Hessel, DeGruyter, Berlin, 2014, ch. 3, p. 64.
19 T. Van Gerven, G. Mul, J. Moulijn and A. Stankiewicz, *Chem. Eng. Process.*, 2007, **46**, 781–789.
20 B. Hook, W. Dohle, P. Hirst, M. Pickworth, M. Berry and K. Booker-Milburn, *J. Org. Chem.*, 2005, **70**, 7558.
21 L. Elliot, J. Knowles, P. Koovits, K. Maskill, M. Ralph, G. Lejeune, L. Edwards, R. Robinson, I. Clemens, B. Cox, D. Pascoe, G. Koch, M. Eberle, M. Berry and K. Booker-Milburn, *Chem. – Eur. J.*, 2014, **20**, 15226.
22 J. Schachtner, P. Bayer and A. Jacobi von Wangelin, *Beilstein J. Org. Chem.*, 2016, **12**, 1798–1811.
23 G. Kreisel, S. Meyer, D. Tietze, T. Fidler, G. Gorges, A. Kirsch, B. Schäfer and S. Rau, *Chem. Ing. Tech.*, 2007, **79**, 153.
24 G. Held, *Introduction to Light Emitting Diode Technology and Applications*, CRC Press, Boca Raton, 2009.
25 W. Ehrfeld, V. Hessel and H. Löwe, *Microreactors*, Wiley-VCH, Weinheim, 2000.
26 V. Hessel, A. Renken, J. Schouten and J.-I. Yoshida, *Micro Process Engineering*, Wiley-VCH, Weinheim, 2009.
27 J.-N. Tourvieille, F. Bornette, R. Philippe, Q. Vanderberghe and C. de Bellefon, *Chem. Eng. J.*, 2013, **227**, 182.
28 C. Mallia and I. Baxendale, *Org. Process Res. Dev.*, 2016, **20**, 327.
29 Y. Matsushita, N. Ohbab, S. Kumadab, K. Sakeda, T. Suzuki and T. Ichimura, *Chem. Eng. J.*, 2008, **135S**, S303–S308.
30 S. Fuse, N. Tanabe, M. Yoshida, H. Yoshida, T. Doi and T. Takahashi, *Chem. Commun.*, 2010, **46**, 8722–8724.
31 C. Park, R. Maurya, J. Lee and D.-P. Kim, *Lab Chip*, 2011, **11**, 1941–1945.
32 O. Shvydkiv, A. Yavorskyy, S. Tan, K. Nolan, N. Hoffmann, A. Youssef and M. Oelgemöller, *Photochem. Photobiol. Sci.*, 2011, **10**, 1399–1404.
33 K. Yeong, A. Gavriilidis, R. Zapf and V. Hessel, *Chem. Eng. Sci.*, 2004, **59**, 3491.
34 M. Zanfir, A. Gavriilidis, C. Wille and V. Hessel, *Ind. Eng. Chem. Res.*, 2005, **44**, 1742.
35 H. Zhang, G. Chen, J. Yue and Q. Yuan, *AIChE J.*, 2009, **55**, 1110.

36 M. Al-Rawashdeh, V. Hessel, P. Löb, K. Mevissen and F. Schönfeld, *Chem. Eng. Sci.*, 2008, **63**, 5149.
37 H. Ehrlich, D. Linke, K. Morgenschweis, M. Baerns and K. Jähnisch, *Chimia*, 2002, **56**, 647.
38 K. Jähnisch and U. Dingerdissen, *Chem. Eng. Technol.*, 2005, **28**, 426.
39 O. Shvydkiv, C. Limburg, K. Nolan and M. Oelgemöller, *J. Flow Chem.*, 2012, **2**, 52.
40 T. H. Rehm, S. Gros, P. Löb and A. Renken, *React. Chem. Eng.*, 2016, **1**, 636.
41 R. Zapf, G. Kolb, H. Pennemann and V. Hessel, *Chem. Eng. Technol.*, 2006, **29**, 1509–1512.
42 E.-Y. Kim, D. Kim and B.-T. Ahn, *Bull. Korean Chem. Soc.*, 2009, **30**, 193–196.
43 Reaction plates with ZnO and Bi_2O_3 as immobilized metal oxides were prepared by the same method as the reaction plate carrying TiO_2.
44 T. H. Rehm, C. Berguerand, S. Ek, R. Zapf, P. Löb, L. Nikoshvili and L. Kiwi-Minsker, *Chem. Eng. J.*, 2016, **293**, 345–354.
45 N. Steinfeldt, R. Abdallah, U. Dingerdissen and K. Jähnisch, *Org. Process Res. Dev.*, 2007, **11**, 1025–1031.
46 M. van Dam, J.-P. Corriou, N. Midoux, A. Lamine and S. Roizard, *Chem. Eng. Sci.*, 1999, **54**, 5311.
47 E. Dikio, S. Nelana, D. Isabirye and E. Ebenso, *Int. J. Electrochem. Sci.*, 2012, **7**, 11101–11122.
48 R. Zapf, C. Becker-Willinger, K. Berresheim, H. Bolz, H. Gnaser, V. Hessel, G. Kolb, A.-K. Pannwitt and A. Ziogas, *Trans. IChemE.*, 2003, **81A**, 721–729.